Eur. Phys. J. B **5**, 495–503 (1998)

THE EUROPEAN PHYSICAL JOURNAL B

d + s wave superconductivity: Analysis of the electronic Raman data of $YBa_2Cu_3O_{7-\delta}$ and other cuprates*

R. Nemetschek[1], R. Hackl[1], M. Opel[1], R. Philipp[1], M.T. Béal-Monod[2,a], J.B. Bieri[2], K. Maki[3], A. Erb[4], and E. Walker[4]

[1] Walther Meissner Institut, Bayerische Akademie des Wissenschaften, 85748 Garching, Germany
[2] Physique des Solides, Université Paris-sud, 91400 Orsay, France
[3] Department of Physics and Astronomy, U.S.C., Los Angeles, CA 90089-0484, USA
[4] Departement de Physique de la Matière Condensée, Université de Genève, 24 quai E. Ansermet, 1211 Genève 4, Switzerland

Received: 3 March 1998 / Accepted: 30 April 1998

Abstract. After briefly recalling the $d+s$ model valid for some anisotropic high T_c superconductors, we present a theory of electronic Raman spectra in that model and then compare it with new experimental data obtained for an overdoped Y123 single crystal. The $d+s$ model appears to describe satisfactorily the experimental results, indicating a possible doping dependence of the mixing ratio. We note that the Raman spectrum of the overdoped Bi2212 could also be accounted for by the $d+s$ superconductivity model. The case of Hg1212 (or Hg1223) is reexamined. It appears that the spontaneous breakdown of d-wave symmetry may be rather universal in high T_c cuprates.

PACS. 74.72.-h High-T_c compounds – 78.30.-j Infrared and Raman spectra

1 Introduction

Perhaps the most gratifying event after the discovery of high T_c superconductors by Bednorz and Müller [1] is that d-wave symmetry seems now established in hole-doped high T_c cuprates [2,3]. However it is worth noting that the superconductivity of the electron-doped superconductor $Nd_{2-x}Ce_xCuO_4$ appears to be of s-wave type [4,5]. The d-wave symmetry of the order parameter may be tested by the presence of nodes in $\Delta(\mathbf{k})$ seen by ARPES [6], the T-linear dependence of the superfluid density $\rho_S(T)$ [7] and the T^2 dependence of the low temperature part in the specific heat [8,9], the electronic Raman spectrum [10a,b] and the thermal conductivity in a magnetic field within the $a-b$ plane [11,12]. Of course $\Delta(\mathbf{k})$ changes sign four times,going around the c-axis,which is tested by phase sensitive Josephson interferometry experiments [13,14] for the generation of $\phi_0/2$ quantum flux in the center of the tricrystal rings [15]. Indeed the tricrystal experiment appears to be more versatile for this particular problem. In this way, Tsuei, Kirtley and their collaborators established the existence of d-wave like symmetry for Y123, Tl2201, Bi2212 and Hg1212.

In this universal agreement, an early c-axis Josephson tunneling experiment [16] between Y123 and Pb casted a doubt,since this implied at least that the Y123 superconductivity contains an s-wave component [17]. Therefore, for this compound at least, the $d+s$ wave model, whose order parameter is given by

$$\Delta(\mathbf{k}) = \Delta[\cos(2\phi)+r] = \Delta_0\frac{[\cos(2\phi)+r]}{1+|r|} \qquad (1)$$

is very natural [18,19]; we recall that the simplest $d+s$ model requires that $|r|<1/\sqrt{2}$ [20]. Here ϕ is the angle $\mathbf{k}$ (in the $a-b$ plane) makes with the a axis. Very recently the validity of the above $d+s$ model was confirmed in a similar Josephson tunneling experiment but with a single twin in Y123 under the tunneling junction [21]. We recall that the shape of the $d+s$ gap (1), with $|r|<1/\sqrt{2}$, is a four leaf clover with the size of the leaves in one direction being different from the size of the leaves in the perpendicular direction, so that the nodes are not at $\pi/4$, like in the pure d-wave case (see the Appendix A).

So far the $d+s$ model has been tested only with Y123 single crystals. From the $a-b$ anisotropy of the magnetic penetration depth [22], a value of $r=-0.3$ could be deduced [18b]. On the other hand,the splitting of the peak in the electron density of states observed by Maggio-Aprile *et al.* [23] gives $|r|=0.25$. Furthermore, we believe that the distortion of the vortex lattice from a tilted square as seen by SANS [24] and STM [23] is due to the s-wave component in the $d+s$ wave superconductivity. Both the study of the quasiparticle spectrum around a single vortex [25] and the rhombic vortex lattice [26] suggests that the

* Dedicated to J. Zittartz on the occasion of his 60th birthday.

[a] e-mail: zazie@hprib.lps.u-psud.fr

vortices are aligned along the nodal directions of $\Delta(\mathbf{k})$. If this is the case,we would have $r = -0.29$ and -0.22 from SANS and STM data respectively. s contributions of this order of magnitude have also been inferred from the Raman spectra of Y123 [27]. In this last publication only the low energy part of the spectra has been considered, but $|r|$ was probably overestimated since the quasi-particle damping was ignored [27b]. Indeed one of the important questions to be answered is whether the low frequency linear term in the B_{1g} spectrum is due to the s-wave component in the $d+s$ model or simply to the quasi-particle damping [27b]. To do this, a systematic analysis of, at least, the A_{1g}, B_{1g} and B_{2g} spectra, as done here, is required. Very recently, the temperature dependence of the phonons in untwinned Y123 has been studied by Raman scattering [28]. There are clear differences between the xx and the yy polarized spectra which are also suggestive of $d+s$ mixing.

In the following, we will first present the theoretical expressions of the electronic Raman spectrum for hybrid pairing superconductivity at $T = 0$ K. Although the Raman spectra expressions in the $d+s$ model have been given elsewhere [29] and applied to Hg1212 compounds, it contained some errors which we will correct here. Then the experimental procedure and the Raman spectra for the Geneva Y123 crystals, with different doping levels are given. In Section 4 we summarize these results and add the reanalysis of the Raman data for Hg1212 (or Hg1223). We find that the Raman spectra from the optimally doped and the overdoped Y123 are fully consistent with $d+s$ wave superconductivity with $|r| \leq 0.15$ and with a reasonable amount of the quasiparticle damping. Also, surprisingly, we find an excellent description of the Raman spectra from overdoped Bi2212 with the $d+s$ model with $|r| \leq 0.3$, which increases with oxygen doping. Even the Hg1212 (or Hg1223) data can be fitted with a considerable amount of damping and with $|r| \sim 0.1$. Of course a symmetry argument [30] forbids $d+s$ wave superconductivity in tetragonal crystals like the Bi and Hg compounds. Perhaps we are witnessing here the breakdown of the tetragonal (or pure d-wave) symmetry.

2 Formalism

The Raman spectra in $d+s$ wave superconductivity are expressed in terms of the Tsuneto function [31]:

$$\lambda = \lambda' + i\lambda'' \tag{2}$$

$$\lambda' = \frac{4\Delta^2(\mathbf{k})}{\omega\sqrt{4\Delta^2(\mathbf{k})-\omega^2}}\tan^{-1}\left(\frac{\omega}{\sqrt{4\Delta^2(\mathbf{k})-\omega^2}}\right) \times \theta[4\Delta^2(\mathbf{k})-\omega^2] + \frac{4\Delta^2(\mathbf{k})}{\omega\sqrt{\omega^2-4\Delta^2(\mathbf{k})}} \times \frac{1}{2}\ln\left(\frac{\omega-\sqrt{\omega^2-4\Delta^2(\mathbf{k})}}{\omega+\sqrt{\omega^2-4\Delta^2(\mathbf{k})}}\right)\theta[\omega^2-4\Delta^2(\mathbf{k})] \tag{3}$$

$$\lambda'' = \frac{\pi}{2\omega}\frac{4\Delta^2(\mathbf{k})}{\sqrt{\omega^2-4\Delta^2(\mathbf{k})}}\theta[\omega^2-4\Delta^2(\mathbf{k})]. \tag{4}$$

We recall that the Tsuneto function was well-known in superfluid ^{3}He [32a], charge density and spin density wave [32b] and even d-wave superconductivity [32c] before the Raman studies.

For the $d+s$ model, $\Delta(\mathbf{k})$ is given in equation (1) and we will use: $\omega = 2\Delta_0 x$. Then the spectra (for $i = A_{1g}, B_{1g}$ and B_{2g}) are given by:

$$S_i = \mathrm{Im}\left\{\langle\gamma_i^2\lambda\rangle - \frac{\langle\gamma_i\lambda\rangle^2}{\langle\lambda\rangle}\right\} \tag{5}$$

where $\langle ...\rangle$ means the average over the angle and the Raman vertices are:

$$\gamma_{A_{1g}} = \sqrt{2}\frac{\varepsilon\cos(2\phi)+\cos(4\phi)}{\sqrt{1+\varepsilon^2}},$$
$$\gamma_{B_{1g}} = \sqrt{2}\cos(2\phi),\ \gamma_{B_{2g}} = \sqrt{2}\sin(2\phi). \tag{6}$$

In principle, in $\gamma_{B_{1g}}$ and $\gamma_{B_{2g}}$, there is also an additive constant term but it is easy to show that the contribution of this term vanishes identically. The vertices are given for tetragonal symmetry with small orthorhombic distortions. This changes the (tetragonal) A_{1g} vertex in a way that a twofold component is to be added which is then the lowest order A_{1g} expansion function. Therefore the magnitude of ε cannot easily be estimated. It turns out, however, that the $\cos(2\phi)$ and $\cos(4\phi)$ contributions are additive and, for simplicity, we will set $\varepsilon = 0$ in the following. We will also drop higher order harmonics like $\cos(8\phi)$... It is well-known that, in the pure d-wave case [10], the screening (*i.e.* the second term in Eq. (5)) enters only in A_{1g}, while for the $d+s$ case, both the A_{1g} and the B_{1g} screenings are crucial, while the B_{2g} screening term vanishes identically. This feature appears to be unique to the $d+s$ model, among possible proposed candidates for high T_c superconductivity like $d+is$ and $d+g$ for instance. Unfortunately this feature was missed in reference [29a]. The theoretical curves for B_{1g}, B_{2g} and A_{1g} are shown in Figure 1 for various $|r|$ values: $r = 0$ (d model), $|r| = 0.1$ and 0.3 ($d+s$ model).

Within the $d+s$ model (1) and in the small ω or x limit (neglecting the constant ε in Eq. (6)), we get from (5):

$$S_{A_{1g}} \approx \frac{\pi}{2}\frac{(2r^2-1)^2}{\sqrt{1-r^2}}(1+|r|)x,$$
$$S_{B_{1g}} \approx \frac{\pi}{2}\frac{r^2}{\sqrt{1-r^2}}(1+|r|)x, \tag{7}$$
$$S_{B_{2g}} \approx \frac{\pi}{2}\sqrt{1-r^2}(1+|r|)x.$$

It is worth noticing that the screening term does not play any role in the x linear terms in formulas (7); it contributes only to higher order terms. Note also that the low x linear dependence of B_{1g}, present in the $d+s$ model, vanishes with r and thus does not arise in the d-wave model whose B_{1g} spectrum starts with a cubic term [31].

Aside from the variation with frequency of the Raman spectra in the $d+s$ model, for $(1+|r|)x \ll 1$ and $(1+|r|)x \gg 1$, we can evaluate analytically all the integrals involved at $x = 1$ and $x = (1-|r|)/(1+|r|)$.

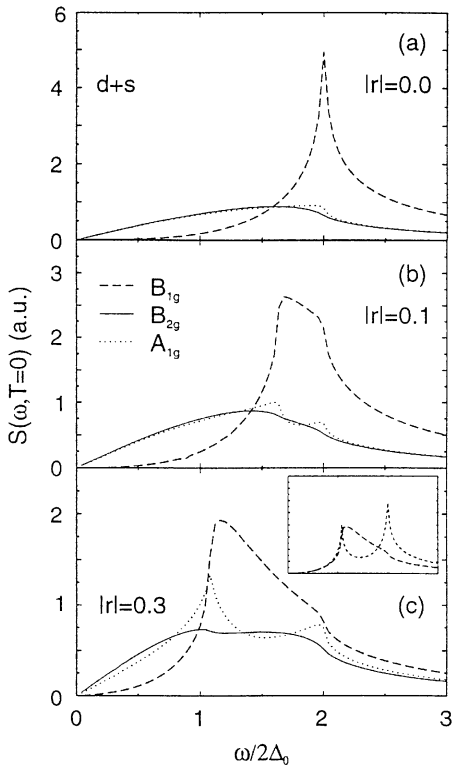

Fig. 1. Theoretical prediction for the B_{1g}, B_{2g} and A_{1g} Raman spectra for the $d+s$ model as given in the text in equation (1) for a cylinder-like Fermi surface and different $|r|$ values. A very small damping $\gamma = \Gamma/(2\Delta_0) = 0.006$ has been added to the frequency in order to control the integrals. The inset in (c) shows the effect of screening in B_{1g} symmetry (short dashed: unscreened). For $|r| = 0.3$ all peaks are essentially at the same position well below the maximum gap energy $2\Delta_0$.

This shows that the logarithmic singularities are completely eliminated from the Raman spectra of A_{1g} and B_{1g}, yielding only single finite peaks in both spectra. It has been suggested earlier [29] that the Raman spectra of the optimally doped Y123 [10b,33,34] are more consistent with the $d+s$ model rather than the pure d-wave one.

In the following, the experimental details will be presented concerning the Raman spectra of Y123. Then we discuss the results and reanalyze the spectra of the Hg compounds [35].

3 Experiments

The experiments were performed in back-scattering geometry using a double monochromator with single-channel detection and the resolution set at $8\,\mathrm{cm}^{-1}$. For excitation the Ar^+ line at 476 nm was selected. The maximal power was 4 mW in order to keep the laser-induced heating below 15 K. The beam was focused to a spot of approximately $50 \times 150\,\mu\mathrm{m}^2$. For the study of the excitations we were interested in, the polarizations of the incoming and outgoing photons were always parallel to the planes. The coordinate system is locked to the Cu-O bonds with $x = [100]$, $x' = [110]$, *etc.* All symmetries refer to a tetragonal point group. B_{1g} phonons and the continuum are projected out with $x'y'$ polarization. Excitations transforming like A_{1g} cannot be accessed independently and are seen with contributions of B_{1g} and B_{2g} type whenever the polarizations are parallel.

Table 1. Approximate positions of the pair-breaking maxima.

	oxygen doping	7.0	6.93	6.5
	$T_c(K)$	87	92	~ 54
$\omega_{peak}(\mathrm{cm}^{-1})$	B_{1g}	470	550	*
	B_{2g}	380	400	220
	A_{1g}	380	400	*

(* not observed [40]).

Since the orthorhombic distortion in Y123 favors the $d+s$ mixing, this compound will be in the main focus of the present paper. The crystals were grown in $BaZrO_3$, which has been shown to be completely inert and to facilitate the preparation of samples with a purity of better than 99.995% [36]. All crystals were post annealed in pure oxygen and quenched. Temperatures and oxygen partial pressures were adjusted according to the calibration of Lindemer *et al.* [37]. The resulting oxygen concentrations were 6.5, 6.93 and very close to 7.0 for the samples that we call under-doped, optimally doped and over-doped, respectively, in the following. The magnetically determined respective T_c values (transition widths δT_c) were 53.5 K (δT_c = 3 K), 91.5 K (δT_c = 0.3 K) and 87.0 K (δT_c = 1.0 K). From the frequency of the apex-oxygen vibration the doping level of the samples can be checked independently [38] to an accuracy of approximately ± 0.03. The respective numbers are 6.53, 6.93 and 6.96. For the highest doping level it cannot be excluded that, at least at the surface, the desired content of 7.0 could not be maintained during the course of the experiments. The transition width after the experiments was indeed larger by almost a factor of 3.

Results for the optimally doped and the overdoped samples are shown in Figures 2 and 3. The spectra at the B_{1g} and B_{2g} symmetries are raw data while the A_{1g} contributions have been obtained by substracting the xy (B_{2g}) spectra from the $x'x'$ $(A_{1g} + B_{2g})$ data. All phonons are generally included. Well pronounced pair- breaking peaks are found in all symmetries (see Figs. 2 and 3), the positions of which are listed in Table 1. Since the transition temperatures of the two samples differ by less than 5 K, one would not expect serious differences in the spectra [39]. However the B_{1g} pair-breaking feature is shifted by more than 20% downwards in the overdoped sample as already found by Chen *et al.* [34b]. The B_{2g} and the A_{1g} maxima seem to scale roughly with T_c in agreement with results for other doping levels in Y123 [40] and Bi2212 [41]. The experiments and the subsequent fits to the data have a twofold purpose: (i) to check the maximum admixture of an s component to the predominant d symmetry of the gap, and (ii) to look for an explanation

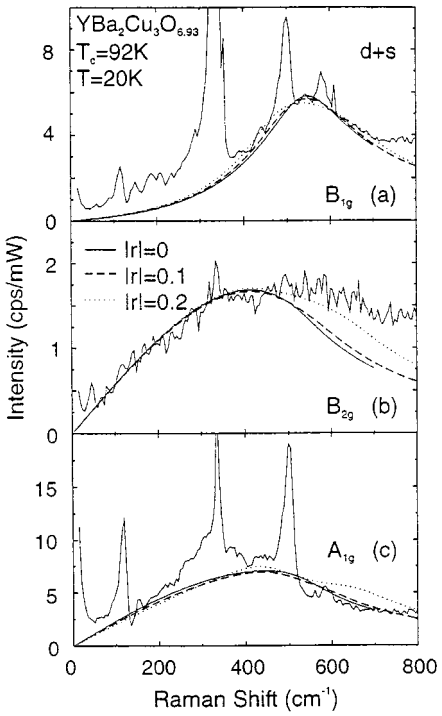

Fig. 2. Experimental data for the B_{1g}, B_{2g} and A_{1g} spectra for optimally doped Y123 and theoretical curves for the $d+s$ model for various $|r|$ values. To account for finite resolution and quasiparticle lifetime a small damping $\gamma = 0.12$ has been added. An admixture of an s component up to $|r| = 0.1$ is compatible with the data. Then $2\Delta_0/T_c = 9.3$. Larger mixing leads to discrepancies in both the B_{2g} and A_{1g} spectra and to exceedingly large values of $2\Delta_0/T_c$ up to 11 for $|r| = 0.2$.

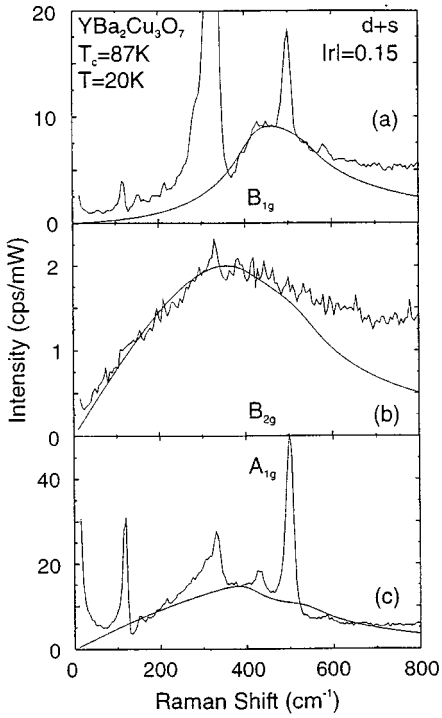

Fig. 3. Experimental data for the B_{1g}, B_{2g} and A_{1g} spectra for overdoped Y123 and theoretical curves for the $d+s$ model. Here $\gamma = 0.06$ and $2\Delta_0/T_c = 9.0$. While the B_{2g} and the A_{1g} peaks scale essentially with T_c [40,41] the B_{1g} maximum moves to lower energies much faster. This can be explained with increasing $|r|$ for higher doping levels. As one can visualize from (c), $|r| = 0.15$ seems to be the biggest admixture compatible with the Raman spectra.

Table 2. Fitting parameters used for the differently doped Y123 samples.

	$\Delta_0(\mathrm{cm}^{-1})$	$\lvert r\rvert$	$\Delta(\mathrm{cm}^{-1})$	$2\Delta_0/T_c$	γ
underdoped (6.5)	175	0	175	8.5	0.14
(T_c 60 K)					
opt. doped (6.93)	275	0	275	8.5	0.13
($T_c = 92$ K)	300	0.1	273	9.3	0.12
	340	0.15	283	10.6	0.10
overdoped (7.0)	275	0.15	240	9.0	0.06
($T_c = 87$ K)					

of the downshift of the B_{1g} maximum in the overdoped sample which exceeds the magnitude expected from T_c by a factor of 4. Since fits using a pure d-wave model have already been presented [42], we check here the compatibility of small s contributions to the gap. In Figure 2, fits with $r = 0$, $r = 0.1$ and $r = 0.2$ are shown. The respective parameters are listed in Table 2. The phonons have not been substracted as two of them depend strongly on temperature and are normalized in the superconducting state [42,43]. Nevertheless the qualitative trends are seen immediately. It turns out that, for the optimally doped sample, a 10% admixture of an s component is still compatible with the data while 20% leads to a serious deviation in the spectral shape in the B_{2g} and A_{1g} symmetries. Here a broadening of $\gamma = \Gamma/(2\Delta_0) = 0.12$ has been used in order to account for finite resolution and quasiparticle damping of not specified origin. Therefore the linear part at low energies is strongly enhanced as compared to the theoretical curves with small damping (Fig. 1). As the accuracy of the data is not sufficiently high for a quantitative comparison of the response in the limit $\omega \to 0$, such as in Bi2212 [41b], we do not have to worry about the actual size of the broadening. In the overdoped sample, a much better fit can be obtained with a higher s contribution of $|r| = 0.15$ (Fig. 3 and Tab. 2). If r is chosen this way, the maximum gap energy $2\Delta_0/T_c$ is, once again, of the order 9 as at all other doping levels (Tab. 2). We note that this is a possible explanation not only for Y123 but also for heavily overdoped Bi2212 where all pair-breaking maxima are at the same position [41] which can be obtained with $|r| = 0.3$ (see Fig. 1). The problem with Bi2212 is that $d + s$ is not compatible with the symmetry of the distortion in this compound, if it occurs in the way one would expect from the superstructure in the BiO_2 layers [44]. This subject has to be clarified before a fit to those data is justified.

4 Discussion

In this section, we discuss that Raman spectra obtained for the Geneva Y123 crystals, the overdoped Bi2212 sample, and we reanalyze the Saclay Hg1212 (or Hg1223) crystal data.

4.1 Overdoped and optimally doped YBCO

First of all, the Raman spectra at the B_{1g}, B_{2g} and A_{1g} symmetries from the overdoped Y123 crystal are well described by $d + s$ superconductivity with $\Delta_0 = 276\,\mathrm{cm}^{-1}$ (397 K), $|r| = 0.15$ and $\Gamma/(2\Delta_0) = 0.06$ as seen from Figure 3.

A similarly good fit is done for optimally doped Y123 with $\Delta_0 = 300\,\mathrm{cm}^{-1}$ (431 K), $|r| = 0.1$ and $\Gamma/(2\Delta_0) = 0.13$. But we see clearly that $|r| = 0.2$ cannot fit B_{1g}, B_{2g} and A_{1g} consistently (see Fig. 2). Therefore, except for the fact that we need a somewhat larger damping, the Raman spectra from the optimally doped Y123 is fully consistent with the $d+s$ model. Earlier STM data from the optimally doped Geneva Y123 crystal [23] gave $\Delta_0 = 350$ K and $|r| = 0.22$ to 0.25 (see Sect. 1). Therefore the Raman data may suggest a somewhat larger Δ_0 and smaller $|r|$. But we do not consider this as a serious discrepancy, since the effect of the damping was not introduced in the earlier theoretical analysis of the STM data [18b]. Also we note that the Geneva Y123 crystal has consistently smaller $|r|$ values (~ 0.2) than the other Y123 crystals ($|r| \sim 0.3$ as seen in Ref. [18b]). We note that Strohm and Cardona [27] find fairly large values, $0.2 < |r| < 0.4$, which are, however, not compatible with the full spectra (see Fig. 1).

4.2 Optimally and overdoped Bi2212

According to reference [30], there will be no symmetry reason that the $d+s$ model applies to the overdoped Bi2212. Furthermore the diagonal distortion on the crystal surface seen by STM on Bi2212 [44] rather suggests a $d+g$ pairing. But both the observed electron density of states [44] and the present Raman data do not support this possibility. On the other hand, the $d+s$ model with $2\Delta_0/T_c = 8.5$ and $0 \leq |r| \leq 0.3$ (with $r = 0$ at the optimally doped Bi2212 and small damping, (*i.e.* $\Gamma/(2\Delta_0) \leq 0.1$) could describe very well the observed Raman spectra.

The approximate constancy of Δ_0/T_c for different oxygen dopings is very intriguing. It does not only hold for samples close to optimal doping but seems to work also for fairly low doping levels (see Tab. 2). At first sight, this appears to be similar to what is obtained for pure d-wave superconductivity in the presence of impurities in the unitarity limit [45], where $\Delta(\Gamma_{im}, 0)/T_c(\Gamma_{im}) =$ constant and Γ_{im} is the quasiparticle scattering rate due to impurities. But we cannot extract $\Delta(\Gamma_{im}, 0)$ from the Raman data. Therefore in spite of the symmetry question, it appears that the $d + s$ superconductivity provides the best model to describe the Raman spectra of the overdoped Bi2212. Also the continuous increase of $|r|$ with the oxygen doping in that compound is quite parallel to what happens in the Y123 case.

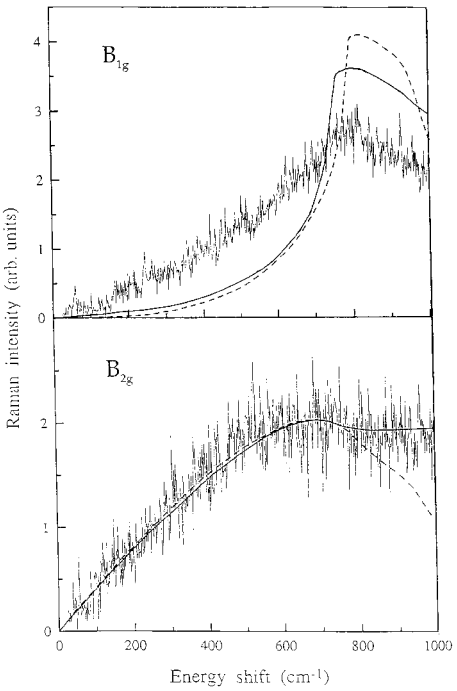

Fig. 4. Reanalysis of the Raman spectra on Hg1212/Hg1223 of references [35] within the $d + s$ model with (dashed line) $|r| = 0.1$ and (full line) $|r| = 0.3$. Here only a very small damping has been added ($\gamma = 0.008$).

4.3 Reanalysis of the Raman spectra from Hg1212 (or Hg1223)

The very same Raman spectra were presented in references [35a,b], once for Hg1212 and the other time for Hg1223. Indeed, chemically [46], one always gets a mixture of both phases. In reference [29a] the Raman spectra were analyed using the $d + s$ model since the $g + s$ model presented in references [35a,b] cannot be reconciled with the tricrystal experiment of Tsuei [47]. On the other hand, the Hg compounds are, at least on the average, tetragonal, and $d + s$ pairing is not allowed. Therefore, in reference [29a] a possible breakdown of d-wave symmetry was proposed. However three points are missing in reference [29a]: (i) the Coulomb screening term, crucial in the B_{1g} spectrum, was forgotten [29b]. Indeed such a term eliminates the two logarithmic singularities of the unscreened B_{1g} spectrum and produces a single and finite broad peak, which is more consistent with the experimental data; (ii) the possible rescaling of the amplitudes of the different spectra, coming from band structure effects [31], was not considered. A reanalysis of the spectra of reference [35], which incorporates these two points is shown in Figure 4 for $|r| = 0.1$ and 0.3 and a rescaling factor of 2/3 for B_{1g}. It is clear that such a reanalysis is not satisfactory: we need a too large value of $|r| = 0.3$ to reach a very good fit for B_{2g},

Table 3. $d+s$ fitting parameters used for Hg1212/Hg1223.

$\Delta_0\,(\mathrm{cm}^{-1})$	$\lvert r\rvert$	$\Delta\,(\mathrm{cm}^{-1})$	$2\Delta_0/T_c$	γ
400	0	400	9.1	0.2
440	0.1	400	10.0	0.2

although the fit for B_{1g} remains poor; in particular, no value of $|r| \leq 0.3$ could account for the large ω linear term of the B_{1g} spectrum. Moreover there is no way to match the peak position of A_{1g} (not shown in Fig. 4) within this approximation. It seems that a large quasiparticle damping must be considered [27b]; (iii) therefore such a damping $\gamma\,(\equiv \Gamma/(2\Delta_0)) = 0.2$ has been introduced in Figure 5 for $r = 0$ and $|r| = 0.1$, yielding a much better fit for all the Raman spectra. The fitting parameters are collected in Table 3. It is interesting that even $r = 0$ (pure d-wave) gives quite a good fit, although the fit with $|r| = 0.1$ looks slightly better particularly in B_{1g} symmetry. Of course there is a small bump in A_{1g}, which is not accounted for by the theory. The shape of the bump, however, suggests that it is due to defect-induced phonons. Contributions from disorder-induced Raman scattering can well be subject to symmetry selection rules and must not show up at all polarizations. In addition, these features are fully consistent with the disorder due to the mixed nature of the Hg1212 / Hg1223 crystals. Reference [35] discarded the presence of impurities as the observed $T_c = 126$ K is rather high. However a careful resistivity measurement and a series of Raman spectra in the normal phase are required to decide this issue. As the Hg-based compounds are apparently a mixture of phases, it is highly desirable to study the single layer compound Hg1201, which, although not free of defects [48], seems to grow as a well-defined phase [46]. In spite of these problems, it seems that the $d+s$ model with a small $|r|$ value of 0.1 describes the Raman spectra of Hg1212 (or Hg1223), if a damping somewhat larger than for the Geneva Y123 crystal is used. If a $g+s$ model is applied with the same vertices γ_i as used here, *i.e.* truncated after $\cos(4\phi)$, the discrepancies with the data are much more serious (see Appendix B).

To summarize, we have analyzed the Raman spectra for Y123, overdoped Bi2212 and Hg1212 (or Hg1223) compounds. All these systems are well described in terms of $d+s$ wave superconductivity with $|r|$ of the order of 0.1, although the symmetry prohibits [30] $d+s$ pairing in Bi2212 and Hg1212 (or Hg1223) unless the tetragonality of these compounds is broken globally or locally. On the other hand, Tl2201 and Hg1201 have the tendency to have a local orthorhombic distortion [48]. Also we have learned that the electronic Raman spectra provide a rather subtle insight into the symmetry of the superconducting order parameter. In another context, the breakdown of d-wave symmetry has been seen in a small circular disk of Tl2201 by a very sensitive magnetotorquemetry experiment [49]. Therefore it is perhaps not so surprising that $d+s$ wave superconductivity works so well in all these different hole doped high T_c cuprates.

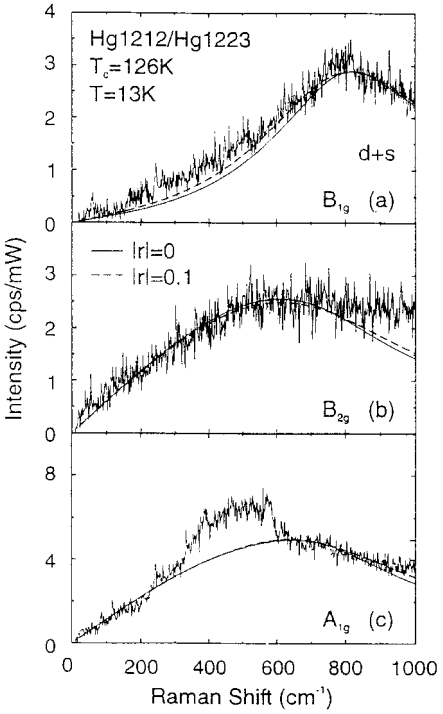

Fig. 5. Reanalysis of the Raman spectra on Hg1212/Hg1223 of references [35] within the $d+s$ model for $|r| = 0.1$ and a bigger damping than in Figure 4, $\gamma = 0.2$.

One of us (K.M.) thanks P. Wyder for his hospitality at LCMI-MPI Grenoble and benefited from useful discussions with H. Won and A. Virosztek; he also acknowledges a NSF grant DMR 95-31720. Two of us (M.T. B.-M. and K.M.) gratefully acknowledge a NATO grant GRG 970267. Finally, all of us are indebted to A. Sacuto for providing his spectra on Hg1212/Hg1223.

Appendix A: d + g and g + d models

We present here some results obtained from the $d+g$ and the $g+d$ models with the gap $\Delta(\mathbf{k})$ given by:

$$\Delta(\mathbf{k}) = \Delta[\cos(2\phi) + r\sin(4\phi)]. \qquad \text{(A.1)}$$

The $d+g$ model (for $|r| < 0.5$) is likely to be the case if the crystal distortion is in the diagonal direction as is the modulation occuring in the Bi2212 compound [44]. On the other hand, the $g+d$ model (for $|r| > 0.5$) would appear unphysical, at least if one is only concerned by small deviations from d-wave superconductivity.

As shown in Figures 6 and 7, the gap shape for $d+g$ exhibits 4 leaves for $|r| < 0.5$ and 8 leaves for $|r| > 0.5$, with a two-fold symmetry with respect to the diagonal in both cases (as compared with the two-fold symmetry with respect to the axis in the $d+s$ model that we show here in Figure 8 for $|r| = 0.2$ for comparison). Figures 6 and 7 illustrate this with $|r| = 0.2\,(d+g)$ and $|r| = 0.7\,(g+d)$. The four leaf structure, $|r| < 0.5$, is consistent with

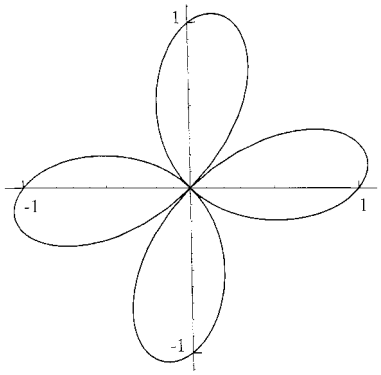

Fig. 6. The gap shape for the $d + g$ model of equation (A.1) for $|r| = 0.2$.

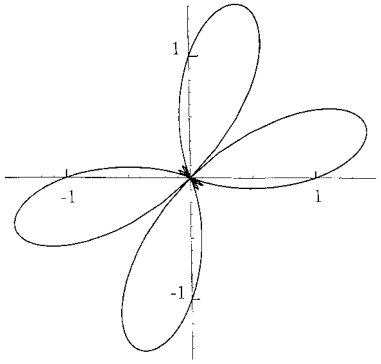

Fig. 7. The gap shape for the $g + d$ model of equation (A.1) for $|r| = 0.7$.

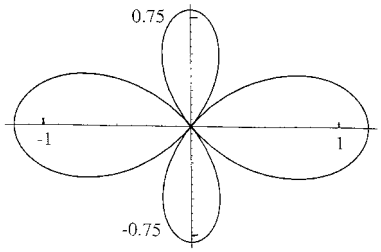

Fig. 8. The gap shape for the $d + s$ model of equation (1) for $|r| = 0.2$.

the Tsuei's experiment [15] and the eight leaf one, $|r| > 0.5$, may still be as exhibiting odd numbers of nodes per quadrant.

We will now present first the theoretical Raman spectra in Figure 9 for $|r| = 0.2$ and 0.7. A linear initial slope in B_{1g} appears only in the unphysical region $|r| > 0.5$, while, for $|r| < 0.5$, B_{1g} always starts with a cubic term in x. For $|r| = 0.2$, B_{1g} exhibits a peak, while B_{2g} and A_{1g} have broad maxima; in contrast, for $|r| = 0.7$ (the unphysical region), B_{1g} exhibits a second maximum at very low energy where B_{2g} and A_{1g} are also both peaked. Such a feature arises also in the density of states as shown below.

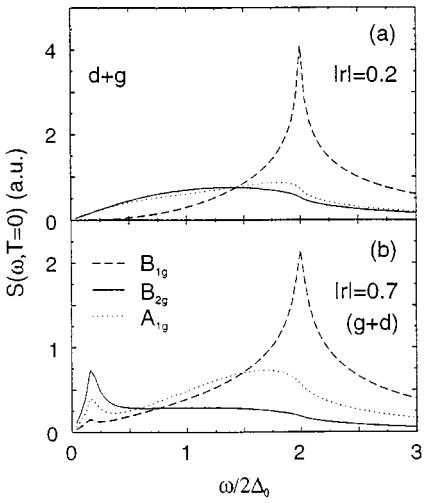

Fig. 9. Theoretical prediction for the B_{1g}, B_{2g} and A_{1g} Raman spectra in the $d+g$ model ($|r| = 0.2$) and with the $g+d$ model ($|r| = 0.7$). Here a very small damping $\gamma = 0.006$ has been used. A small g component, $|r| = 0.2$ as one might expect for Bi2212 would be compatible with the experimental data,while a big one, $|r| = 0.7$ can be excluded.

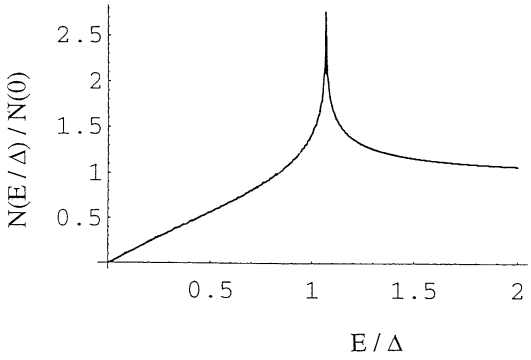

Fig. 10. The density of states for the $d+g$ model for $|r| = 0.2$.

We note also that the screening term in (5) plays a role in B_{2g} but vanishes in B_{1g}, contrary to the $d + s$ model.

The density of states curves are shown in Figures 10 and 11 for two values of $|r|$. It is given by:

$$\frac{N(E/\Delta)}{N(0)} = \int_0^{2\pi} \frac{d\phi}{2\pi} \mathrm{Re}\left[\frac{E/\Delta}{\sqrt{(E/\Delta)^2 - [\cos(2\phi) + r\sin(4\phi)]^2}}\right]. \quad \text{(A.2)}$$

$N(0)$ is the normal state density of states at the Fermi energy and is supposed to be a constant here. $N(E/\Delta)/N(0)$ exhibits one peak for $|r| = 0.2$ and two peaks for $|r| = 0.7$. It is interesting to compare these results with the density of states found in reference [20] for, respectively, the $d+s$ model with $|r| = 0.1$ (see Fig. 16 in Ref. [20]) and a $s+d$ model with $|r| = 0.9$ (see Fig. 14 in Ref. [20]). The only difference is that, for small $|r|$ values, the $d + s$ density

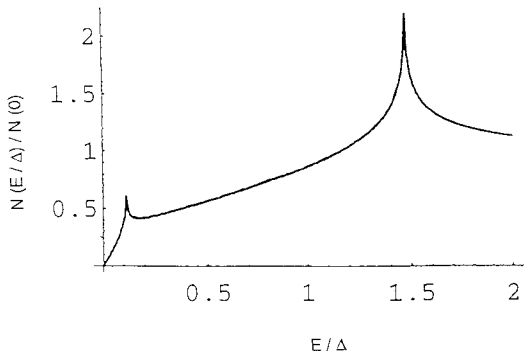

Fig. 11. The density of states for the $g+d$ model for $|r| = 0.7$.

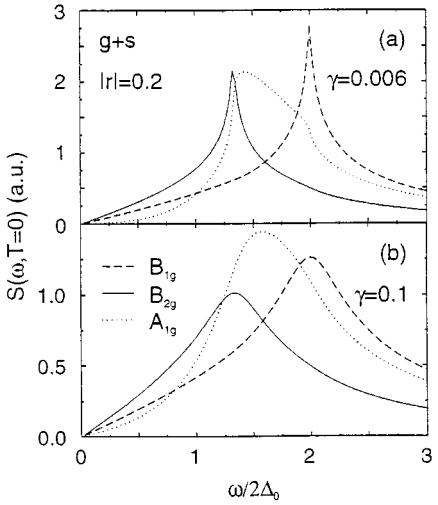

Fig. 12. Theoretical curves for the $g + s$ model presented in reference [35] for the B_{1g}, B_{2g} and A_{1g} Raman spectra and for different damping values γ, (a) $\gamma = 0.006$, (b) $\gamma = 0.1$.

of states exhibits two peaks, while the $d + g$ one has only one peak. This comes from the fact the the $d+s$ gap shape has leaves of two different sizes (Fig. 8), while those in the $d + g$ model are of equal size (Fig. 6).

For the time being, we are not aware of any specific experimental data which could correspond to such behaviors. However we found it useful to give here the theoretical predictions, in comparison with the $d+s$ and $s+d$ models of reference [20].

Appendix B: Raman spectra in the g + s model

As an alternative to d or $d + s$ superconductivity, an extended s-wave model has been proposed in references [35] for the interpretation of the data for Hg1212 (Hg1223). We prefer not to call this order parameter an extended s-wave, but rather $g+s$, since the g-component is dominant. This $g + s$ gap varies as

$$\Delta(\mathbf{k}) = \Delta_0 \frac{\cos(4\phi) + r}{1 + |r|} \cdot \tag{A.3}$$

For convenience the theoretical calculations for the respective Raman spectra are reproduced here for different damping values $\gamma = \Gamma/(2\Delta_0) = 0.006$ and 0.1 and $|r| = 0.2$ (Fig. 12). In contrast to reference [35], the expansion of the Raman vertices is truncated after $L = 2$ (or $\cos(4\phi)$), for the A_{1g} symmetry. In this model, the B_{1g} and B_{2g} spectra should exhibit the same shapes. In addition, the A_{1g} spectrum is much broader than the theorerital prediction and in the wrong place. Finally, the low frequency variation of the data seems to be better reproduced for the $d(+s)$ model. Although we need a relatively large damping to account for the linear low-energy part of the B_{1g} spectrum (which, however, is comparable to that used in Refs. [35]), we feel the d-wave superconductivity cannot at all be excluded for the Hg compounds. The Raman data can rather be understood quite well in the $d + s$ scenario.

References

1. J.G. Bednorz, K.A. Müller, Z. Phys. B **64**, 189 (1986).
2. See for instance Proc. Int. Conf. Low Temp. Phys., Prague (1996) in Czech; J. Phys. **46**, Suppl. S1-6, (1996); Proc. Int. Conf. M2S-HTSC-V, Beijin (1997) in Physica B **282-287**, (1997).
3. D.J. Scalapino, Phys. Rep. **250**, 329 (1995); K. Maki, H. Won, Ann. Phys. (Leipzig) **5**, 320 (1996); J. Phys. France **6**, 2317 (1996).
4. P.H. Wu *et al.*, Phys. Rev. Lett. **70**, 85-88 (1993); S.M. Anlage *et al.*, Phys. Rev. B **50**, 523 (1993).
5. B. Stadlober *et al.*, Phys. Rev. Lett. **74**, 4911 (1995).
6. Z.X. Shen *et al.*, Phys. Rev. Lett. **70**, 1553 (1994); H. Ding *et al.*, Phys. Rev. Lett. **50**, 1333 (1994).
7. W.H. Hardy *et al.*, Phys. Rev. Lett. **70**, 3989 (1993).
8. K.A. Moler *et al.*, Phys. Rev. Lett. **73**, 2744 (1994).
9. N. Momono *et al.*, Physica C **233**, 395 (1994).
10. a) T.P. Devereaux *et al.*, Phys. Rev. Lett. **72**, 396 (1994); b) For a review see R. Hackl in *The Gap symmetry and fluctuations in high T_c superconductors*, NATO ASI, Cargese (1997), edited by J. Bok, G. Deutscher, D. Pavuna, S.A. Wolf (Plenum Press, 1998).
11. M.B. Salomon *et al.*, J. Superconductivity **8**, 449 (1995); Yu Fang *et al.*, Phys. Rev. Lett. **77**, 3059 (1996).
12. H. Aubin *et al.*, Phys. Rev. Lett. **78**, 2024 (1997).
13. D.A. Wollman *et al.*, Phys. Rev. Lett. **71**, 2134 (1993); Phys. Rev. Lett. **74**, 797 (1995).
14. D.A. Brawner, H.R. Ott, Phys. Rev. B **50**, 6530 (1996); Phys. Rev. B **53**, 8249 (1996); A. Mathai *et al.*, Phys. Rev. Lett. **74**, 4523 (1995).
15. C.C. Tsuei *et al.*, Phys. Rev. Lett. **73**, 593 (1994); J. Kirtley *et al.*, Nature **373**, 225 (1996); C.C. Tsuei *et al.*, Science **271**, 329 (1996); Europhys. Lett. **36**, 707 (1996).
16. A.G. Sun *et al.*, Phys. Rev. Lett. **72**, 2267 (1994); **76**, 2161 (1996).
17. M. Sigrist, T.M. Rice, Rev. Mod Phys. **67**, 503 (1995).

18. a) M.T. Béal-Monod, O.T. Valls, Physica C **235-240**, 2145 (1994); Europhys. Lett. **30**, 415 (1995); b) M.T. Béal-Monod, K. Maki, Phys. Rev. B **55**, 1194 (1997) and earlier references therein; c) K. Maki, M.T. Béal-Monod, Phys. Rev. B **55**, 11730 (1997); d) M.T. Béal-Monod, Physica C **298**, 59 (1998).
19. H. Kim, E. Nicol, Phys. Rev. B **52**, 13576 (1995).
20. M.T. Béal-Monod, K. Maki, Phys. Rev. B **53**, 5775 (1996).
21. K.A. Kouznetsov *et al.*, Phys. Rev. Lett. **79**, 3050 (1997); M.E. Zhitomirsky, M.B. Walker, Phys. Rev. Lett. **79**, 734 (1997).
22. K. Zhang *et al.*, Phys. Rev. Lett. **73**, 2484 (1994); D.N. Basov *et al.*, Phys. Rev. Lett. **74**, 598 (1995).
23. I. Maggio-Aprile *et al.*, Phys. Rev. Lett. **75**, 2754 (1995).
24. B. Keimer *et al.*, Phys. Rev. Lett. **73**, 3459 (1995).
25. Y. Morita, M. Kohmoto, K. Maki, Phys. Rev. Lett. **78**, 4841 (1997); Europhys. Lett. **70**, 207 (1997).
26. J. Shiraishi, M. Kohmoto, K. Maki (to be published).
27. a)T. Strohm, M. Cardona, Sol. State Commun. **104**, 233 (1997); b) T.P. Devereaux, Phys. Rev. Lett. **74**, 4313 (1995).
28. M.F. Limonov *et al.*, Phys. Rev. Lett. **80**, 825 (1998).
29. a) M.T. Béal-Monod, J.P. Bieri, K. Maki, Europhys. Lett. **40**, 201 (1997); b) Erratum, Eur. Phys. Lett. **41**, 345 (1998).
30. J.F. Annett *et al.*, J. Low Temp. Phys. **105**, 473 (1996).
31. T.P. Devereaux, D. Einzel, Phys. Rev. B **51**, 16336 (1995).
32. a) H. Ebisawa, K. Maki, Progr. Theor. Phys. **51**, 337 (1987); b) A. Virosztek, K. Maki, Phys. Rev. B **35**, 1954 (1987); K. Maki, A. Virosztek, Phys. Rev. B **48**, 1368 (1987); c) K. Maki, H. Won, Phys. Rev. Lett. **72**, 1758 (1994); H. Won, K. Maki, Phys. Rev. B **49**, 15305 (1994).
33. R. Hackl *et al.*, Phys. Rev. B **38**, 7133 (1988).
34. a) S.L. Cooper *et al.*, Phys. Rev. B **38**, 11934 (1988); b) X.K. Chen *et al.*, Phys. Rev. B **48**, 10530 (1993).
35. a) A. Sacuto *et al.*, Europhys. Lett. **39**, 207 (1997); b) A. Sacuto, R. Combescot in *The Gap symmetry and fluctuations in high T_c superconductors*, NATO ASI, Cargese (1997), edited by J. Bok, G. Deutscher, D. Pavuna, S.A. Wolf, Plenum (to be published).
36. A. Erb *et al.*, Physica C **282-287**, 89 (1997).
37. T.B. Lindemer *et al.*, J. Am. Ceram. Soc. **71**, 1775 (1992).
38. R. Feile, Physica C **159**, 1 (1989).
39. R. Hackl *et al.*, SPIE (Bellingham) **2696**, 194 (1996).
40. R. Nemetschek *et al.*, Phys. Rev. Lett. **78**, 4837 (1997).
41. a) C. Kendziora, A. Rosenberg, Phys. Rev. B **52**, 9867 (1995); b) R. Hackl *et al.*, J. Low Temp. Phys. **105**, 733 (1996).
42. T.P. Devereaux *et al.*, Phys. Rev. B **51**, 505 (1995).
43. C. Thomsen, in *Light scattering in solids*, Topics in Appl. Phys. **68**, 285 (Springer, Berlin, Heidelberg, 1991).
44. C. Renner, Ø. Fischer, Phys. Rev. B **51**, 9208 (1995); M. Oda *et al.*, Phys. Rev. B **53**, 2253 (1996).
45. Y. Sun, K. Maki, Phys. Rev. B **51**, 605 (1995); Europhys. Lett. **32**, 355 (1995).
46. V. Viallet, Ph.D. thesis, Orsay, France, 1998, unpublished; A. Bertinotti *et al.*, in *Studies of High Temperature Superconductors* **23**, edited by A. Narlikar (Nova Sciences Publishers, New York, 1997) pp. 27-85.
47. C.C. Tsuei, private communication (1997); J.Y.T. Wei *et al.*, Phys. Rev. B **57**, 3650 (1998).
48. J.D. Jorgensen *et al.*, Physica C **282-287**, 97 (1997).
49. C. Rossel *et al.*, Physica C **282-287**, 136 (1997); M. Willemin *et al.*, Phys. Rev. B **57**, 6137 (1998).